



Electrochemical behaviors and determination of rifampicin on graphene nanoplatelets modified glassy carbon electrode in sulfuric acid solution

Jiao Zou, Le-Le Huang, Xin-Yu Jiang, Fei-Peng Jiao, Jin-Gang Yu*

College of Chemistry and Chemical Engineering, Central South University, Changsha, Hunan 410083, China, Tel. +86 731 88879616, email: zoujiao@csu.edu.cn (J. Zou), 1805228971@qq.com (L.-L. Huang), jiangxinyu@csu.edu.cn (X.-Y. Jiang), jiaofp@163.com (F.-P. Jiao), yujg@csu.edu.cn (J.-G. Yu)

Received 18 December 2017; Accepted 4 July 2018

ABSTRACT

In this work, a novel electrochemical sensor based on graphene nanoplatelets (GNPs) film was designed and prepared to detect rifampicin. GNPs were dispersed in deionized-distilled water, and the suspension was modified onto the surface of glassy carbon electrode (GCE) by a drop-coating process. Cyclic voltammetry (CV) and differential pulse voltammetry (DPV) were used to investigate the electrochemical behaviors of rifampicin on modified electrode with GNPs (GNPs/GCE). Several factors affecting the current response of rifampicin, including the types and concentration of support electrolyte solutions, the volume of GNPs solutions were investigated. Under the optimized conditions, the proposed GNPs/GCE showed a good response and recognition effect for rifampicin in sulfuric acid electrolytes. In the range of 10^{-3} μ M to 100 μ M, the modified electrode could achieve a good linear effect with a good coefficient of determination ($R^2 = 0.996$), and the limit of detection reached 0.5 nM. It could be used as a simple, fast and sensitive electrochemical sensor system for the detection and quantification of rifampicin.

Keywords: Electrochemical sensor; Graphene nanoplatelets; Rifampicin; Differential pulse voltammetry

1. Introduction

The widespread use of antibiotics has caused serious problems of bacterial resistance, which has gradually threatened the health of humans and other organisms [1,2]. On the other hand, the abuse of antibiotics can even induce antibiotic resistant bacteria [3]. Drug monitoring plays an important role in drug quality control and has a great impact on public health [4]. Rifampicin (RIF), 3-[(4-methyl-1-piperazinyl) imino] methyl rifamycin (Fig. 1) belongs to the class of macrocyclic antibiotics, and it is one of the most effective tuberculostatic agents against mycobacterium strains. RIF has been used for the treatment of several serious infectious such as tuberculosis, leprosy and HIV [5]. RIF has also been widely used in the treatment of a variety of bacterial infections, although it can cause some adverse effects such as nausea, liver poisoning, and allergic rash. The mechanism of drug function is related to RIF's ability

of inhibiting bacterial DNA-dependent RNA polymerase [6]. Due to the essential effect on numerous pathological processes of RIF, various methods have been developed to detect and quantify RIF, such as enzyme-linked immunosorbent assay (ELISA) [7], capillary electrophoresis (CE) [8], ultraviolet visible spectrophotometry (UV) [9,10], liquid chromatography (LC) [11,12], wireless magnetoelastic-sensing device [13], flow-injection chemiluminescence [14] and voltammetry [15], electrochemical sensing [16], and other integrated methods. For ELISA, it is difficult to prepare antibody, detect small or unstable compounds and realize high selectivity. CE and UV were not highly sensitive and reproducible, therefore, they should be equipped with highly sensitive detectors and the samples need to be pretreated. LC was susceptible to matrix interference, baseline drift, and multiple interference peaks, especially in the detection of complex systems. The wireless magnetoelastic-sensing device was greatly affected by magnetic fields and a strict detection environment was usually required [13]. It is very difficult to select a suitable chemilumines-

*Corresponding author.

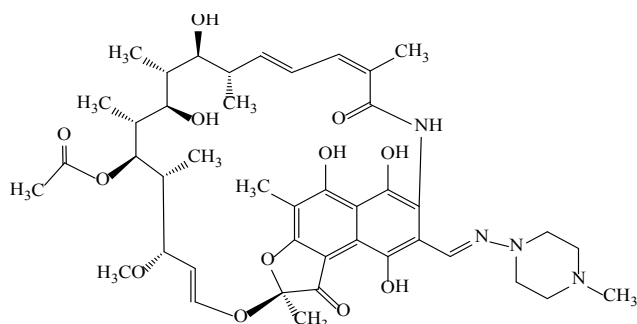


Fig. 1. Chemical structure of RIF.

cent reagent for flow-injection chemiluminescence method although it seems more sensitive [14]. The voltammetry is not a very accurate method and the systematic error was relatively large. For many of the reported technologies, extensive pre-purification, time-consuming and complex equipment are the main realistic limitations. Obviously, highly operational, fast, effective, and selective analytical techniques for determining RIF are expected.

Due to their high sensitivity, low cost, simplicity, stability, miniaturization, less time-consuming and environment-friendly, electrochemical methods have aroused considerable interest [17]. With the increasing development of modified electrodes, the reactivity, sensitivity and selectivity of the electrochemical methods have been greatly improved. Recently, a variety of materials such as surfactant, metal nanoparticles [18,19], carbon materials, and conducting polymers [20] have been used to modify electrodes and applied to detect RIF.

In recent years, the application of carbon nanomaterials in the electrochemical sensor has attracted great attention [21–28]. As the basis of carbon-based nanomaterials, graphene is a one-atom-thick carbon nanomaterial which is composed of sp^2 -bonded carbon atoms arranged in a two-dimensional (2D) honeycomb lattice [29–32]. Due to the high specific surface area (theoretical monolayer graphene $2630 \text{ m}^2 \text{ g}^{-1}$), unique morphology [31,33–36], a large number of edges and defects in the planar, high electron transfer rate ($15,000 \text{ cm}^2 \text{ V}^{-1} \text{ s}^{-1}$), high structural stability, strong mechanical strength, excellent thermal conductivity and electrical conductivity, graphene is an ideal material for electrochemical sensing and biosensing [37–39]. Graphene oxide (GO) possesses abundant oxygen-containing functional groups such as hydroxyl, epoxy, carboxyl and carbonyl due to the chemical exfoliation of layered flake graphite using potassium permanganate (KMnO_4) and strong acids including sulfuric acid (H_2SO_4) and phosphoric acid (H_3PO_4) [40–42]. The damaged extended sp^2 conjugate network can be seen on the surface of GO. Graphene nanoplatelets (GNPs) can be manufactured in large scale and less structural damages are generated to their graphitic structures [43,44]. Compared with GO, GNPs possess better electrical conductivity and higher temperature corrosion resistance. And the combination of GNPs with other materials would obtain composites with some novel properties such as high conductivity, good dispersibility, and prominent thermal stability [16]. For example, Rastgar et al. have fabricated nickel hydroxide nanoparticles-reduced graphene oxide

$[\text{Ni}(\text{OH})_2\text{-rGO}]$ modified GCE by a layer-by-layer electrochemical deposition method for highly sensitive sensing of RIF in aqueous solution [45]. However, the procedure for the preparation of the modified electrode was relatively complex, costly and time consuming. As a consequence, it is still necessary to develop simple, sensitive and accurate methods for fabricating novel modified electrodes. The fabrication of modified GCE by the drop-coating process was relatively more facile, faster, more time-saving and stable, which has attracted more and more attention in recent years [46,47].

In the present work, we developed a simple and versatile electrochemical sensor for sensitive detection of RIF. GNPs were dispersed in deionized-distilled water, and the suspension was modified onto the surface of GCE by a drop-coating process to obtain GNPs modified GCE (GNPs/GCE) (Fig. 2). The GNPs and GO were both characterized by Fourier transform infrared (FTIR) spectroscopy, Raman spectroscopy, scanning electron microscopy (SEM), transmission electron microscopy (TEM) and X-ray photoelectron spectroscopy (XPS). Cyclic voltammetry (CV) and differential pulse voltammetry (DPV) were used to investigate the electrochemical behaviors of RIF on GNPs/GCE. Impressively, GNPs/GCE exhibits good electrochemical performance and superior stability in sulfuric acid electrolytes. The experimental conditions are optimized, and the response of RIF on GNPs/GCE is also studied in detail. The fabricated GNPs/GCE could be used for detection of RIF in capsule with very low relative standard deviation.

2. Experimental

2.1. Chemicals and reagents

Graphene Nanoplatelets (GNPs) with purity of 99.5 wt.%, thickness of 4–20 nm, and diameters of 5–10 μm , were purchased from Chinese Academy of Sciences Chengdu Organic Chemistry Co., Ltd. (Chengdu, China). RIF (95% purity) was provided by Shanghai Chemical Reagent Co., Ltd. (Shanghai, China). Phosphoric acid (H_3PO_4), concentrated sulfuric acid (H_2SO_4), concentrated nitric acid (HNO_3), acetic acid (CH_3COOH), sodium dihydrogen phosphate dehydrate ($\text{NaH}_2\text{PO}_4 \cdot 2\text{H}_2\text{O}$), disodium hydrogen phosphate dodecahydrate ($\text{Na}_2\text{HPO}_4 \cdot 12\text{H}_2\text{O}$), Boric acid (H_3BO_3) and methanol were obtained from Sinopharm Chemical Reagent Co., Ltd. (Shanghai, China). Alumina polishing powder was bought from Lab Testing Technology Co., Ltd. (Shanghai, China). Potassium ferricyanide ($\text{K}_3\text{Fe}(\text{CN})_6$) was supplied by Tianjin Broadcom Chemical Co., Ltd. (Tianjin, China). Sodium hydroxide (NaOH) was purchased from Beijing Chemical Works. (Beijing, China) All reagents were of analytical grade and used without further purification. The aqueous solutions were freshly prepared using double distilled water. Stock solution of RIF (1.0 mM) by adding a small amount of methanol dissolved with ultra-pure water constant volume. The working solutions were prepared by diluting the stock solution with 0.1 M sulfuric acid. In these experiments, RIF capsules (0.15 g per capsule) were acquired from China Pharmaceutical Group Wuhan ZoomlionSiyao Pharmaceutical Co., Ltd. (Wuhan, China). Each sample was measured three times in parallel and the relative standard deviation (RSD) was calculated. Electrochem-

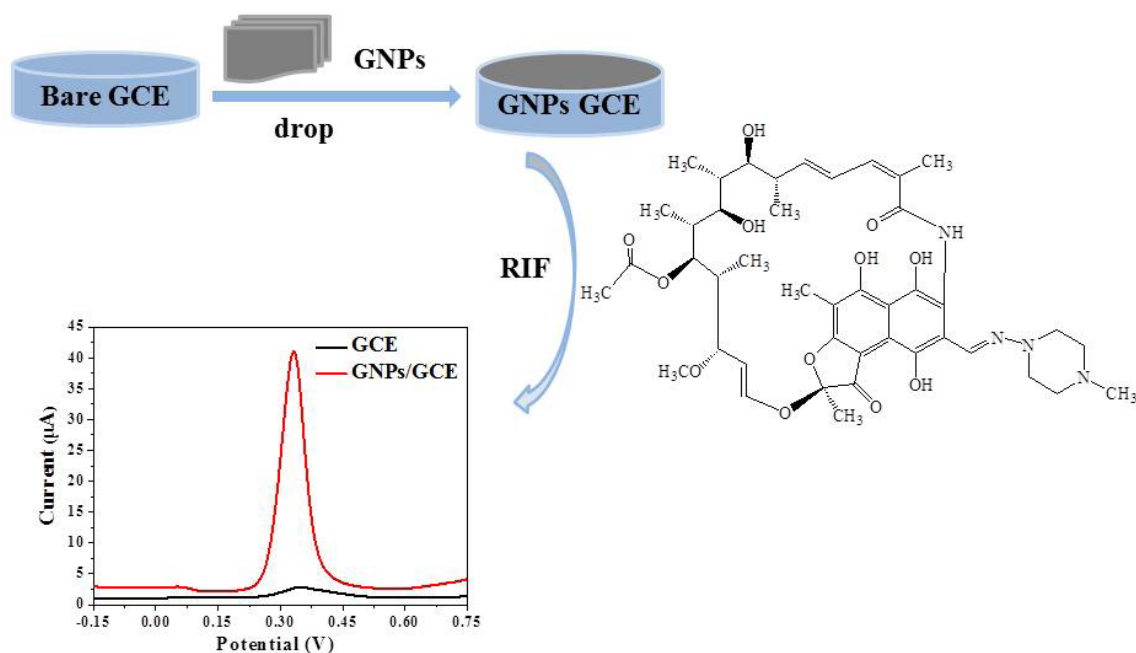


Fig. 2. The preparation of GNPs/GCE and the electrochemical behaviors of RIF on the GNPs/GCE.

ical experiments were performed in sulfuric acid solution (H_2SO_4 , 0.1 M) as the supporting electrolyte. GO was prepared according to the previously reported method by our group [48–50].

2.2. Characterization

The morphologies of GO and GNPs were observed on a field emission scanning electron microscopy (FE-SEM, TESCAN MIRA3 LMH/LMU, Czech) and high resolution transmission electron microscopy (HR-TEM, JEM-2100F, JEOL Ltd., Tokyo, Japan). Fourier transform infrared (FT-IR) spectra were collected on a Bruker Model 12 IFS 66v/s spectrophotometer. The functional groups of GO and GNPs were analyzed by FT-IR spectroscopy (Thermo Electron Inc., San Jose, USA), and the powder samples were homogenized with the potassium bromide (KBr) and then pressed into a transparent sheet and scanned in the wavenumber range of $400\text{--}4000\text{ cm}^{-1}$. Raman spectra was collected at room temperature with a LabRAM HR high resolution Raman spectrometer (Horiba–Jobin Yvon) using a He-Ne laser ($\lambda = 632.8\text{ nm}$). The analyses of the chemical components on the sample surfaces were performed on an X-ray photoelectron spectrometer (model 5300, Perkin-Elmer Corp, Instruments Div, Norwalk, Connecticut), and the X-ray photoelectron spectra (XPS) were recorded with Mg or Al X-ray source at the energies of 1486.6 eV or 1253.6 eV, respectively. Electrochemical measurements were performed using a CHI660E Electrochemical Workstation (Chenhua Instrument Co., Ltd. Shanghai, China) with a classical three-electrode system. A glassy carbon electrode (GCE, diameter: 3.0 mm), a saturated Ag/AgCl electrode and a platinum wire were used as the working electrode, the reference electrode, and the counter electrode, respectively.

2.3 Fabrication of GNPs/GCE and GO/GCE

The as-received GNPs were dispersed in water under ultrasonic treatment to form a uniform suspension with the concentration of 2 mg mL^{-1} . Prior to modification, a bare glassy carbon electrode (3 mm of diameter) was carefully polished to form a mirror-like surface with $0.05\text{ }\mu\text{m}$ alumina slurry on micro-cloth pads, and then ultrasonically cleaned in distilled water for 2 min. After the electrode was allowed to dry under a stream of nitrogen (N_2), it was then immersed in 1 mM of $\text{K}_3\text{Fe}(\text{CN})_6$ (containing 0.1 M KCl) and scanned in the potential range from 0 to +0.6 V (vs. Ag/AgCl) until the peak potential separation (E_p) of CV profiles less than 80 mV. And then the GCE was dried again under a N_2 flow. GNPs/GCE modified electrode was prepared by dropping $9\text{ }\mu\text{L}$ of GNPs suspension onto the GCE surface using a micropipette followed by air-drying. And the GO modified glassy carbon electrode (GO/GCE) was prepared in the same manner.

3. Results and discussions

3.1. Characterizations of GNPs

3.1.1. FT-IR spectroscopy

GO and GNPs were characterized with FT-IR spectra (Fig. 3). As we can see in Fig. 3A, the spectrum of GO shows absorption bands at 3402 cm^{-1} , 1734 cm^{-1} , 1620 cm^{-1} and 1114 cm^{-1} , which are ascribed to stretching vibrations of $-\text{OH}$, $\text{C}=\text{O}$ bond of carboxyl groups, $\text{C}=\text{C}$ of the benzene ring, and $\text{C}-\text{O}-\text{C}$ bond of the epoxy groups, respectively. The absorption peak at 1394 cm^{-1} corresponds to the distorting vibration of the $-\text{OH}$ functional group. These characteristic peaks indicate that the surface of the GO contains abundant oxygen-containing functional groups. As shown in Fig. 3B, the spectrum of GNPs shows stretching vibration

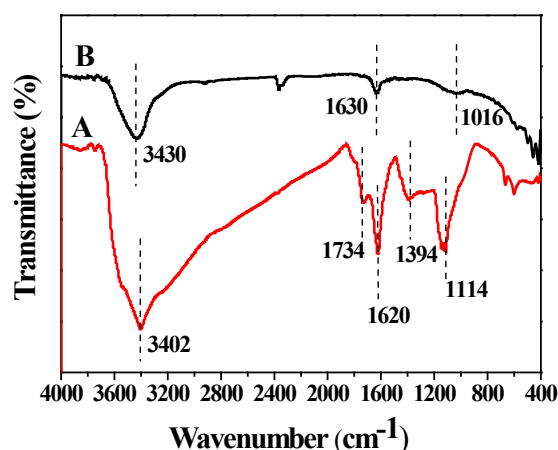


Fig. 3. FT-IR spectra of the materials: (A) GO; (B) GNPs.

of $-OH$ (broad peak at 3430 cm^{-1}), stretching vibration of $C=C$ bond of the benzene ring (at 1630 cm^{-1}), and asymmetrical stretching of $C-O-C$ (at 1016 cm^{-1}). In comparison with GO, the relative intensities of the characteristic absorption peaks of oxygen-containing groups of GNPs decreased dramatically or even disappeared.

3.1.2. Raman spectroscopy

Raman spectroscopy can be used for characterization of surface defects on the carbon nanocomposites. As shown in Fig. 4, GO and GNPs contain two characteristic peaks: the G-band at 1588.2 cm^{-1} represents sp^2 hybrid $C=C$ bonds, and the D-band at 1359.2 cm^{-1} corresponds to the defects or bonded functional groups on the lattice that contain sp^3 hybrid atoms. The intensity ratio (I_D/I_G) of the D-band and G-band was usually used to evaluate the degree of disorder or damage which is a prominent feature in graphene suffering from chemical functionalization. As shown in Fig. 4A, the I_D/I_G of GNPs (0.174) is abruptly decreased compared with that (0.776) of GO, indicating that chemical exfoliation of flake graphite for preparation of GO would generate a mass of defects on the materials.

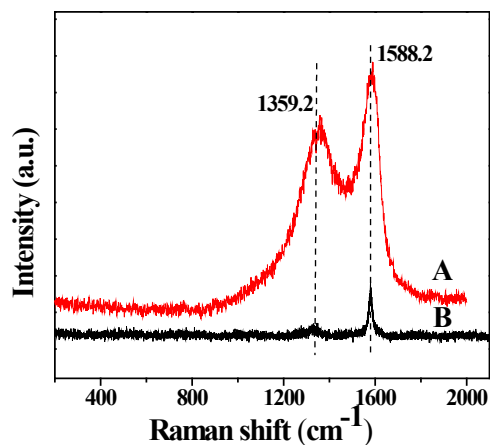


Fig. 4. Raman spectra of the samples: (A) GO; (B) GNPs.

3.1.3. Morphology analysis

The morphological structures of GO and GNPs were investigated by FE-SEM. It can be seen from Fig. 5A that GO possesses a relative smooth planar structure and thin layers, while GNPs consist of multilayers which comprised of many graphite nanosheets (Fig. 5B).

The HR-TEM characterization for GO and GNPs was also carried out. The samples were routinely prepared by pipetting a few milliliters of GO or GNPs dispersion onto holey carbon mesh grids, respectively. The typical HR-TEM images of GO and GNPs are shown in Fig. 5C and 4D, respectively. The stacking sheet structure of GO could be found in the TEM cross-sections, and the individual layer of GO is clearly observed (Fig. 5C). Besides the ordered graphite lattices the disordered regions are also clearly visible, indicating that the GO sheets were partially damaged due to the strong oxidation exfoliation. As for GNPs (Fig. 5D), the ordered graphite lattices are more obvious in the TEM cross-sections, and almost no disordered regions could be found, indicating GNPs possess highly ordered crystal structure.

3.1.4. XPS analysis

X-ray photoelectron spectroscopy (XPS) can be used to qualitatively and quantitatively analyze the surface elements of the materials. The chemical compositions of GO and GNPs were characterized *via* XPS. As shown in Figs. 6A and 6B, it is clear to discern that the relative intensities of the characteristic absorption peaks of oxygen-containing groups of GNPs decreased dramatically or even disappeared (at 533.3 eV), indicating that GNPs appear to contain a low oxygen content (2.5 wt.%) due to the possible removal of oxygen-containing functional groups in the reduction steps of their production process.

3.2 Electrochemical properties of the modified electrodes

To investigate the electrochemical properties of the bare GCE, GNPs/GCE and GO/GCE, cyclic voltammetry (CV) was carried out in $K_3Fe(CN)_6$ solution (1 mM, containing 0.1 M of KCl) with a scan rate of 50 mV s^{-1} in the potential range of $0-0.6\text{ V}$ (vs. $Ag/AgCl$). As shown in Fig. 7A, a couple of oxidation and reduction peaks could be observed at the GNPs/GCE (curve a) with the $\Delta E_p = 80\text{ mV}$, and bare GCE (curve b) with the $\Delta E_p = 65\text{ mV}$, but no redox peak is observed in the CV curve on the GO/GCE. In addition, the peak current on the GNPs/GCE was increased a little in contrast with that on bare GCE. This could be attributed to the excellent electrochemical activity of GNPs, which played an important role in accelerating the electron transport rate of the modified electrodes.

The electrochemical properties of the modified electrodes were determined by electrochemical impedance spectroscopy (EIS). As shown in Fig. 7B, the charge-transfer resistance (R_{ct} , the high frequency intercept of the semi-circle) of bare GCE, GNPs/GCE and GO/GCE are $366.9\ \Omega$, $197.4\ \Omega$, $320\ \Omega$, respectively. The R_{ct} of GNPs/GCE was the lowest, which can be attributed to the excellent electrocatalytic activity, high conductivity and large specific surface area of GNPs. The GNPs exhibited excellent effects on the

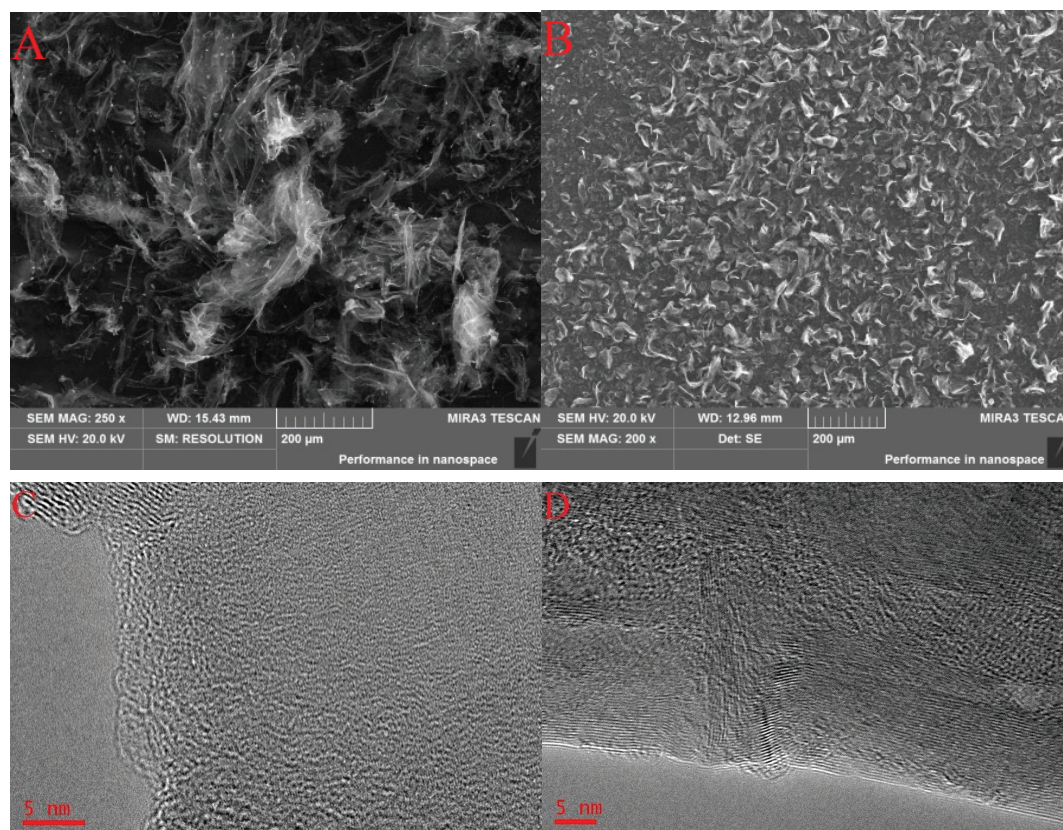


Fig. 5. FE-SEM images of the samples: (A) GO; (B) GNPs; and HR-TEM images of the samples: (C) GO; (D) GNPs.

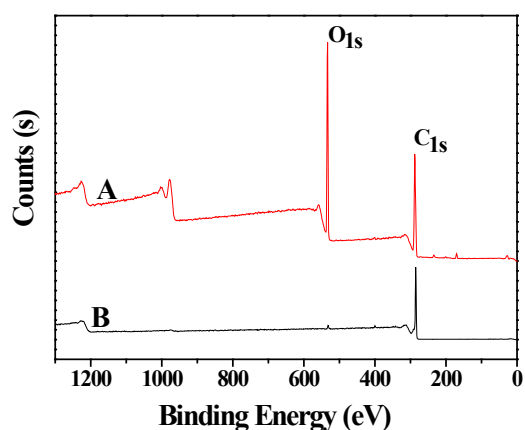


Fig. 6. XPS images of the samples: (A) GO; (B) GNPs.

facilitated electron-transfer reactions in the $K_3[Fe(CN)_6]$ – $K_4[Fe(CN)_6]$ system which are consistent with CVs.

In order to evaluate the electrochemical properties of GNPs/GCE, CVs of the GNPs/GCE in 1 mM $K_3Fe(CN)_6$ solution (containing 0.1 M KCl) at various scan rates (10 – 200 mV s^{-1}) was carried out. As shown in Fig. 7C, the redox peak currents were linearly related to the square root of the scan rate, indicating that the mass transfer onto the electrode surface may be a diffusion control process [51].

As shown in Fig. 7D, differential pulse voltammograms (DPV) of different electrodes were obtained in RIF solution (0.1 mM, containing 0.1 M of H_2SO_4) with the potential range from -0.2 to $+0.8$ V (vs. Ag/AgCl). Compared with the current response of the bare GCE (curve b) in 0.1 mM RIF solution, GNPs/GCE (curve a) showed a higher current response in RIF solution with a peak current of 3.9×10^{-5} A. The current response of GNPs/GCE was enhanced significantly by about 23 times in contrast with that of bare GCE. In contrast, the GO/GCE showed no electrochemical response to RIF probably due to the lower conductivity of GO. We can predict that the GNPs/GCE electrode might have a better detection capability toward RIF.

3.3. Optimization of experimental conditions

3.3.1. The effects of supporting electrolyte

Supporting electrolytes generally play an important role in improving the conductivity of the solutions. It was reported that RIF had higher electrochemical response under the acidic conditions, and the DPV curves of RIF in different acidic electrolytes were investigated experimentally. Electrochemical determination of 0.1 mM of RIF on GNPs/GCE in 0.1 M H_2SO_4 , H_3PO_4 , HNO_3 , CH_3COOH , PBS (pH 4.0), HAc–NaAc (pH 4.0), BR (0.04 M, pH 4.0) and without support electrolyte solutions was investigated, respectively. As we can see in Fig. 8, the peak current of RIF in deionized water was very low (curve h). In the presence of

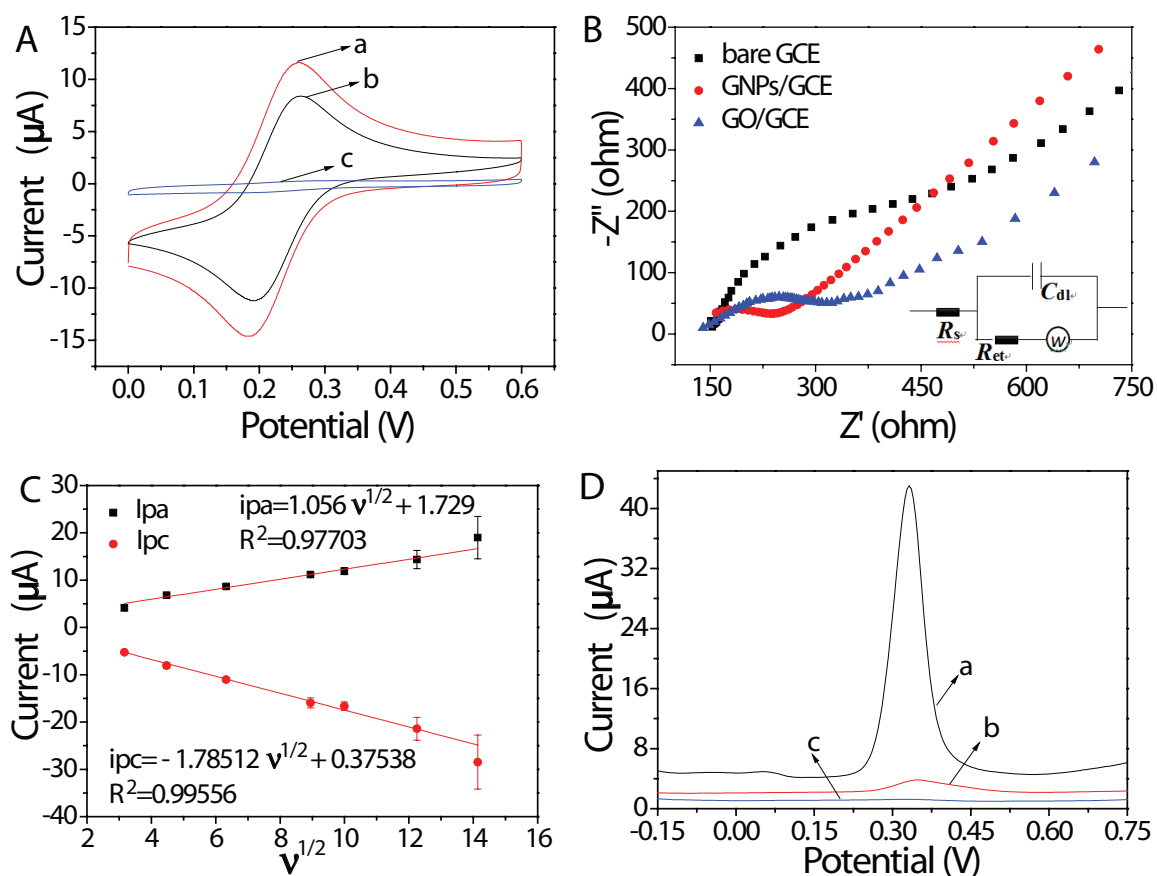


Fig. 7. (A) CV of different electrodes in 1 mM of $\text{K}_3\text{Fe}(\text{CN})_6$ solution (containing 0.1 M of KCl), scan rate 50 mV s^{-1} : (a) GNPs/GCE; (b) bare GCE; (c) GO/GCE. (B) Nyquist plots of different electrodes in 1 mM $\text{K}_3\text{Fe}(\text{CN})_6$ solution (containing 0.1 M KCl) at open-circuit potential conditions (AC frequency range: 0.01 Hz to 10 kHz; AC amplitude: 5.0 mV). (C) Plots of the GNPs/GCE in 1 mM $\text{K}_3\text{Fe}(\text{CN})_6$ solution (containing 0.1 M KCl) redox peak currents as a function of scan rates ($10 - 200 \text{ mV s}^{-1}$). (D) DPV of different electrodes in 0.1 mM of RIF solution (0.1 M of H_2SO_4 as supporting electrolyte): (a) GNPs/GCE; (b) bare GCE; (c) GO/GCE.

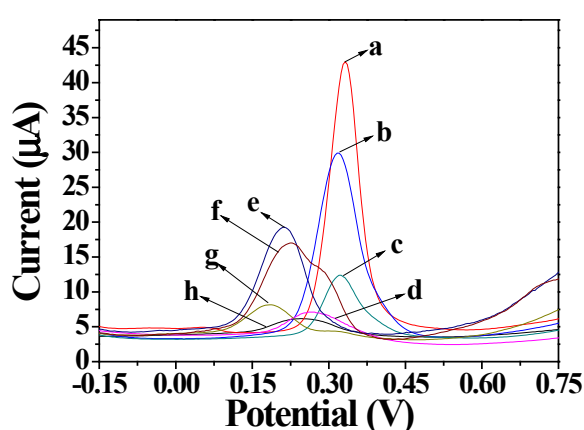


Fig. 8. DPV for RIF (0.1 mM) on GNPs/GCE electrode in various supporting electrolyte solutions: (a) H_2SO_4 ; (b) H_3PO_4 ; (c) HNO_3 ; (d) CH_3COOH ; (e) PBS; (f) HAc-NaAc; (g) BR; (h) without support electrolyte.

supporting electrolyte solutions (curve a ~ g), indicating that supporting electrolyte accelerated the ion transport rate and enhanced the conductivity of the solution, which

had a significant effect on the detection of RIF. The experimental results showed that the peak shape of DPV curve in 0.1 M sulfuric acid solution was the best and the peak current response is the largest. Consequently, 0.1 M H_2SO_4 was selected as the optimum supporting electrolyte for the determination of RIF. RIF on GNPs/GCE showed an oxidation response of 0.332 V (vs. Ag/AgCl) at 0.1 M H_2SO_4 due to the electroactivity of the hydroquinone group.

3.3.2. The effects of pH

Since the transport of protons and anions was involved in the electrochemical oxidation of RIF, pH value of solution would have great impact on the electrochemical responses of RIF. The effects of the electrolyte concentration varying over the range of 0.01–0.25 M which corresponds to the pH value (1.90–0.56) of the solution on the electrochemical response of 0.1 mM RIF on the GNPs/GCE were investigated. As shown in Fig. 9A and B, the peak current and potential both changed at different pH. The maximum peak current was obtained at H_2SO_4 concentration of 0.1 M (pH 1.04), and then decreased when the H_2SO_4 concentration continued to increase. RIF was protonated and posi-

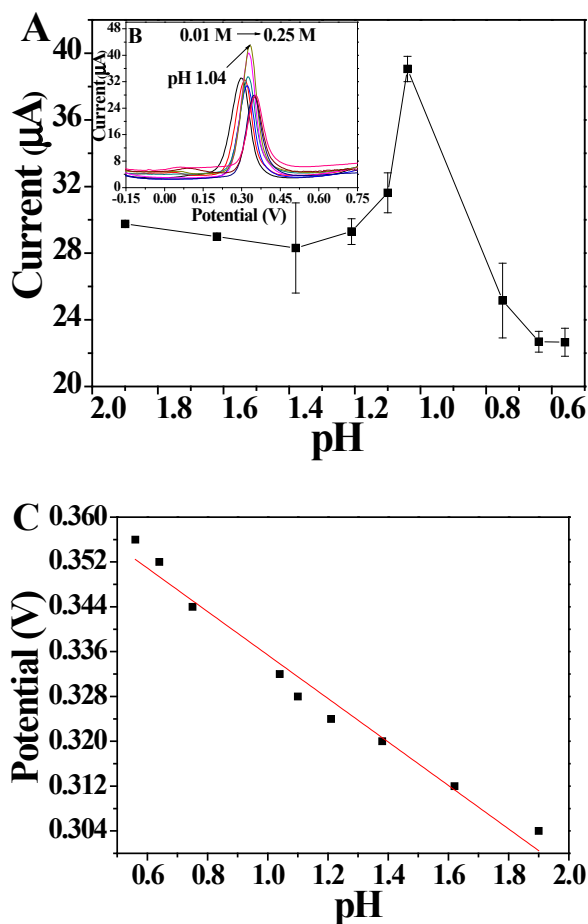


Fig. 9. (A) The effect of pH for 0.1 mM RIF: 1.90, 1.62, 1.38, 1.21, 1.10, 1.04, 0.75, 0.64, 0.56. (B) DPV behaviors of 0.1 mM RIF on the GNP/GCE with different concentration of sulfuric acid: 0.01, 0.02, 0.04, 0.06, 0.08, 0.10, 0.15, 0.20, 0.25 M. (C) The different pH influence on oxidation peak potential of RIF.

tively charged when the acid dissociation constant (K_a) of H_2SO_4 is less than the ionization equilibrium constant (Z^*) of RIF, whereas at the higher H_2SO_4 concentration (>0.15 M) RIF was deprotonated and negatively charged [16]. On the other hand, GNPs were negatively charged due to the great electronic delocalization of the conjugated aromatic rings. The strong electrostatic interactions between GNPs and RIF increased the adsorbed amounts of RIF on the electrode surface, leading to an increasing oxidation peak current. Therefore, 0.1 M H_2SO_4 was used as the optimal electrolyte and used in the following experiments. Furthermore, as we can see in Fig. 9C, oxidation peak potentials of RIF shifted negatively with an increase in pH. The linear regression equations was $E_{pa} (V) = -0.038 \text{ pH} - 0.3742$ ($R^2 = 0.97247$), indicating that the proton was directly involved in the electrochemical redox process of RIF.

3.3.3. The effects of the amount of coated GNPs

The effects of the amount of coated GNPs on the electrochemical response of RIF were investigated. As shown in Fig. 10, the peak current gradually increased to the 10 maximum

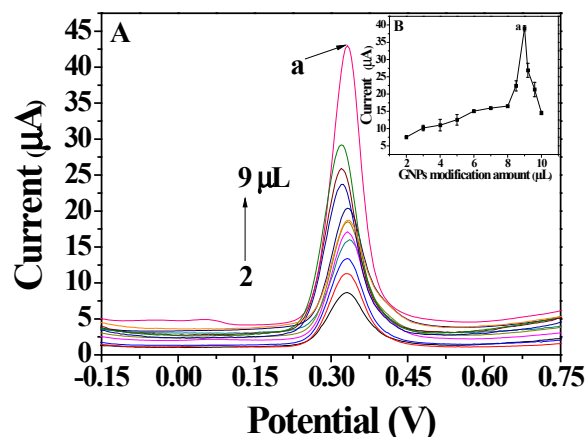


Fig. 10. (A) DPV behaviors of 0.1 mM RIF on the GNP/GCE with different amounts of coated GNPs: 2, 3, 4, 5, 6, 7, 8, 8.5, 9, 9.2, 9.6 and 10 μL (along with the arrow); (B) The effects of amount of coated GNPs for 0.1 mM RIF on the GNP/GCE.

with the amount of coated GNPs gradually increased from 2 μL to 9 μL . While the amount of GNPs was higher than 9 μL , the peak current abruptly decreased. The thickness of the coated GNPs increased remarkably due to the excessive coating GNPs on the GCE, thus deteriorating the conductivity of the GNP/GCE. Moreover, the modified electrode surface slightly overflowed and an uneven coated surface was formed when the amount of the coated GNPs was more than 9 μL . In addition, the electrode surface drying time would also be largely prolonged due to a corresponding increase in the coating amount of GNPs. Therefore, the optimal amount of coated GNPs was set to 9 μL .

3.3.4. Linear range and limit of detection

Under the optimized conditions, DPV analysis of RIF with different concentrations on the GNP/GCE at a scan rate of 50 mV s^{-1} in 0.1 M H_2SO_4 was carried out (Fig. 11A). The peak current was linearly increased with the increase in the RIF concentration, indicating the electrode was extremely sensitivity to detect RIF. Calibration curve (Fig. 11B) for RIF measurement showed a linear relationship to the RIF concentration (0.001–100 μM) with a regression equation of $i_p (\mu\text{A}) = 0.4193 C_{\text{RIF}} + 1.1412$ ($R^2 = 0.996$). As can be seen in Fig. 10C, the peak currents were linear in RIF in concentration range of 0.001–0.5 μM . The detection limit of the sensor for RIF was 0.5 nM. Therefore, GNP/GCE can be used for quantitative analysis of RIF.

To evaluate the selectivity of the proposed sensor, analysis of the influence of some potential interfering species including pharmaceutical formulations and biological fluids that usually coexisted with RIF was performed. It can be seen in Fig. 11D that the peak currents of 2 mM of uric acid, glucose, dopamine, ascorbic acid, L-threonine, D/L-Alanine, D/L-Methionine, L-Tryptophan, L-Glutamine acid and L-Isoleucine would not affect the response signals of RIF (0.04 mM). The low deviations (less than 5.04%) indicated that the proposed GNP/GCE possesses good anti-interference ability.

The stability of GNP/GCE was also tested using the DPV of 0.1 mM RIF in 0.1 M H_2SO_4 . The intra-day precision of GNP/GCE was studied by analyzing RIF for 6 consecu-

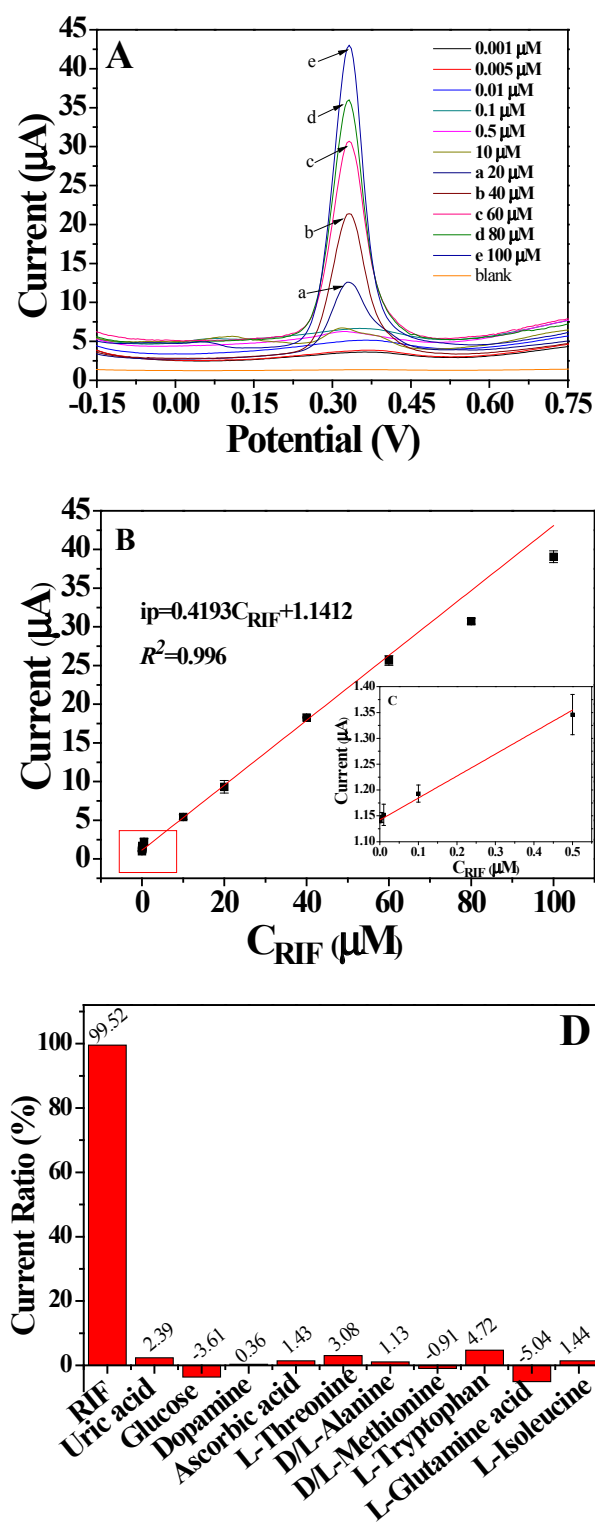


Fig. 11. (A) DPV behaviors of blank and 0.001–100 μM RIF on the GNPs/GCE in 0.1 M H_2SO_4 . (B) Plot of peak current versus RIF concentration. (C) Plot of peak current with the range of 0.001–0.5 μM RIF. (D) The amperometric response current ratios for 0.04 mM RIF with 2 mM of various potential interfering agents (uric acid, glucose, dopamine, ascorbic acid, L-threonine, D/L-Alanine, D/L-Methionine, L-Tryptophan, L-Glutamine acid and L-Isoleucine, respectively) in H_2SO_4 on GNPs/GCE.

five times at the same electrode within one day, the relative standard deviation (*RSD*) of intra-day precise was found to be 0.73%. In addition, the inter-day precision of GNPs/GCE was investigated by determining RIF for 6 times with the same electrode in five successive working days, the *RSD* of inter-day precise was 3.30%. To evaluate the between-run precision, six different batches of electrodes were coated in the same way, and the *RSD* of between-run precision was 2.51%. Therefore, the proposed electrode exhibited good stability and reproducibility for the determination of RIF.

3.3.5. Analytical application to real samples

To investigate the application feasibility of the GNPs/GCE in the determination of RIF, the commercially available RIF capsules were used as the real samples and analyzed. Before analysis, the medicine in a capsule containing 0.1692 g of RIF was transferred into a 250.0 mL volumetric flask, then a small amount of methanol was added for sufficient dissolution, and finally ultra-pure water was gradually added to volume. Precise removal of 1.0 mL of RIF actually in a 10.0 mL volumetric flask, and the solution was then diluted with 0.1 M H_2SO_4 , finally moved into an electrolytic cup. The DPV (Fig. 12) results showed that capsule matrix had no interference effects on the electrochemical analysis of RIF. The quantitative analysis of RIF was repeated three times to determine the DPV peak current, which was calculated by the standard curve equation: $i_p = 0.4194 C_{\text{RIF}} + 1.1412$. The calculated amount of RIF in the capsule was 0.1318 mg with *RSD* of 0.152% ($n = 3$), indicating the fabricated electrode has adequate precision and accuracy, which can meet the needs in practice.

As listed in Table 1, the linearity range, sensitivity, and detection limit of the GNPs/GCE were compared with those previously reported electrodes. Obviously, the detection limit of the GNPs/GCE was almost the lowest except for $\text{CoFe}_2\text{O}_4@\text{CdSe}$ -GCE. However, the fabrication of $\text{CoFe}_2\text{O}_4@\text{CdSe}$ -GCE was relatively more complicated, time-consuming and costly. Therefore, the GNPs fabricated electrodes can be used as potential electrochemical sensors for RIF in practical sample.

In addition, the use of H_2SO_4 rather than phosphate buffered solutions (PBS) as the supporting electrolyte could accelerate the ion transport rate and enhance the conductivity of the solution, which had a significant effect on the

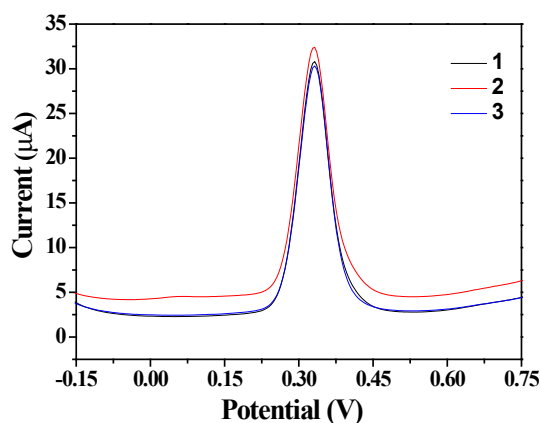


Fig. 12. DPV behaviors of RIF actual sample on the GNPs/GCE.

Table 1
A comparison of the presently reported sensors with the GNPs/GCE

Electrode	Method	Linear range (μM)	LOD (nM)	Ref.
$\text{CoFe}_2\text{O}_4@\text{CdSe}$ -GCE	SWASV ^a	10^{-10} –0.1	4.55×10^{-6}	[16]
$\text{Mn}_3\text{O}_4@\text{SiO}_2$ -CPE	SWV ^b	0.03–3	10.8	[18]
CPE ^c	SWV	0.1–6	17.2	[52]
$\text{Ni}(\text{OH})_2$ -RGO-GCE	LSV ^d	0.006–10	4.16	[45]
GNPs/GCE	DPV	0.001–100	0.5	This work

^aSquare-wave adsorptive anodic stripping voltammetry

^bSquare-wave voltammetry

^cCarbon paste electrode

^dLinear sweep voltammetry

quantitative detection of RIF. To increase the electrochemical recognition sensitivity and resolution, the adopted DPV could also provide more chemical information about the analyte such as its states in complex molecules. Under optimized conditions, the GNPs/GCE gave significantly better peak shape for RIF than that obtained by the $\text{Ni}(\text{OH})_2$ -rGO/GCE. In short, the obtained results indicated that the modified electrode had an excellent capacity for detection of RIF. And the developed GNPs/GCE exhibited many outstanding properties for the electrochemical determination of RIF including lower detection limit, higher sensitivity and wider linearity range. That is to say, GNPs/GCE could be used as a better electrochemical sensor for the quantitative detection and quantification of RIF.

4. Conclusion

In summary, a novel and facile electrochemical sensor based on graphene nanoplatelets film was designed and prepared by a drop coating method, which was successfully used in the quantitative analysis of common antibiotics RIF. CV and DPV were used to investigate the electrochemical behaviors of RIF on the GNPs/GCE. From the DPV curves it can be concluded that the GNPs modified electrode had a good response and recognition performance for RIF in sulfuric acid solution. The modified electrode exhibited high sensitivity and good linear correlation for RIF with a good coefficient of determination (0.996) in the concentration range of 0.001 to 100 μM . The limit of detection reached 0.5 nM. The experimental data were reproducible and the relative standard deviation for RIF in capsule sample was 0.152% under the best experimental conditions. The relatively good properties of the GNPs/GCE foreshadow its broad application for the accurate determination of RIF in pharmaceutical and clinical preparations.

Acknowledgment

The financial supports from National Natural Science Foundation of China (Nos. 51674292 and 21471163), Provincial Natural Science Foundation of Hunan (No. 2016JJ1023) and Project of Innovation-driven Plan in Central South University (No. 2016CX007) are greatly appreciated.

Conflict of Interest: None.

References

- [1] D. Raghunath, Emerging antibiotic resistance in bacteria with special reference to India, *J. Biosci.*, 33 (2008) 593–603.
- [2] C.A. Peloquin, S.E. Berning, Infection caused by *Mycobacterium tuberculosis*, *Annals Pharmacotherapy*, 28 (1994) 72–84.
- [3] L.R. Hoffman, D.A. D'Argenio, M.J. MacCoss, Z.Y. Zhang, R.A. Jones, S.I. Miller, Aminoglycoside antibiotics induce bacterial biofilm formation, *Nature*, 436 (2005) 1171–1175.
- [4] R.O. Laing, H.V. Hogerzeil, D. Ross-Degnan, Ten recommendations to improve use of medicines in developing countries, *Health Policy Plann.*, 16 (2001) 13–20.
- [5] S. Ramaswamy, J.M. Musser, Molecular genetic basis of antimicrobial agent resistance in *Mycobacterium tuberculosis*: 1998 update, *Tubercle Lung Disease*, 79 (1998) 3–29.
- [6] E.A. Campbell, N. Korzheva, A. Mustae, K. Murakami, S. Nair, A. Goldfarb, S.A. Darst, Structural mechanism for rifampicin inhibition of bacterial RNA polymerase, *Cell*, 104 (2001) 901–912.
- [7] L. Garcia, M. Alonso-Sanz, M.J. Rebollo, J.C. Tercero, F. Chaves, Mutations in the *rpoB* gene of rifampin-resistant *Mycobacterium tuberculosis* isolates in Spain and their rapid detection by PCR-enzyme-linked immunosorbent assay, *J. Clin. Microbiol.*, 39 (2001) 1813–1818.
- [8] G.A. Thomas, D.L. Williams, S.A. Soper, Capillary electrophoresis-based heteroduplex analysis with a universal heteroduplex generator for detection of point mutations associated with rifampin resistance in, *Clin. Chem.*, 47 (2001) 1195–1203.
- [9] A.F. Faria, M.V.N. de Souza, R.E. Bruns, M.A.L. de Oliveira, Simultaneous determination of first-line anti-tuberculosis drugs by capillary zone electrophoresis using direct UV detection, *Talanta*, 82 (2010) 333–339.
- [10] S.A. Benetton, E.R.M. Kedor-Hackmann, M.I.R.M. Santoro, V.M. Borges, Visible spectrophotometric and first-derivative UV spectrophotometric determination of rifampicin and isoniazid in pharmaceutical preparations, *Talanta*, 47 (1998) 639–643.
- [11] D.H. Vu, R.A. Koster, M.S. Bolhuis, B. Greijdanus, R.V. Altena, D.H. Nguyen, J.R. Brouwers, D.R. Uges, J.W. Alffenaar, Simultaneous determination of rifampicin, clarithromycin and their metabolites in dried blood spots using LC-MS/MS, *Talanta*, 121 (2014) 9–17.
- [12] F.F. Belal, M.K.S. El-Din, M.I. Eid, R.M. El-Gamal, Micellar HPLC method using monolithic column for the simultaneous determination of linezolid and rifampicin in pharmaceuticals and biological fluids, *Anal. Methods-Uk*, 5 (2013) 6165–6176.
- [13] P. Pang, Q. Cai, S. Yao, C.A. Grimes, The detection of *Mycobacterium tuberculosis* in sputum sample based on a wireless magnetoelastic-sensing device, *Talanta*, 76 (2008) 360–364.
- [14] W. Ruengsitagoon, S. Liawruangrath, A. Townshend, Flow injection chemiluminescence determination of paracetamol, *Talanta*, 69 (2006) 976–983.
- [15] H.Y. Ma, X.W. Zheng, Z. Zhang, Flow-injection electrochemiluminescence detecting rifampicin based on its sensitizing effect, *Chinese J. Chem.*, 22 (2004) 279–282.

- [16] K. Asadpour-Zeynali, F. Mollarasouli, Novel electrochemical biosensor based on PVP capped $\text{CoFe}_2\text{O}_4/\text{CdSe}$ core-shell nanoparticles modified electrode for ultra-trace level determination of rifampicin by square wave adsorptive stripping voltammetry, *Biosens. Bioelectron.*, 92 (2017) 509–516.
- [17] Q. Xia, Y. Huang, X. Lin, S. Zhu, Y. Fu, Highly sensitive D-alanine electrochemical biosensor based on functionalized multi-walled carbon nanotubes and D-amino acid oxidase, *Biochem. Eng. J.*, 113 (2016) 1–6.
- [18] T. Gan, Z. Shi, K. Wang, J. Sun, Z. Lv, Y. Liu, Rifampicin determination in human serum and urine based on disposable carbon paste microelectrode modified with hollow manganese oxide@mesoporous silica oxide core-shell nanohybrid, *Can. J. Chem.*, 93 (2015) 1061–1068.
- [19] N.S.K. Gowthaman, S. Kesavan, S.A. John, Monitoring isoniazid level in human fluids in the presence of theophylline using gold@platinum core@shell nanoparticles modified glassy carbon electrode, *Sensor. Actuat. B-Chem.*, 230 (2016) 157–166.
- [20] T. Gan, Z. Shi, K. Wang, J. Sun, Z. Lv, Y. Liu, Synthesis and characterization of mesoporous tin oxide-functionalized reduced graphene oxide nanoplatelets for ultrasensitive detection of guaiaicol in red wines, *Aust. J. Chem.*, 69 (2016) 220–229.
- [21] J. Ping, Y. Wang, J. Wu, Y. Ying, Development of an electrochemically reduced graphene oxide modified disposable bismuth film electrode and its application for stripping analysis of heavy metals in milk, *Food Chem.*, 151 (2014) 65–71.
- [22] H. Beitollahi, S. Tajik, P. Biparva, Electrochemical determination of sulfite and phenol using a carbon paste electrode modified with ionic liquids and graphene nanosheets: Application to determination of sulfite and phenol in real samples, *Measurement*, 56 (2014) 170–177.
- [23] L. Zhou, J. Wang, D. Li, Y. Li, An electrochemical aptasensor based on gold nanoparticles dotted graphene modified glassy carbon electrode for label-free detection of bisphenol A in milk samples, *Food Chem.*, 162 (2014) 34–40.
- [24] S.Y. Oh, J.G. Son, P.C. Chiu, Black carbon-mediated reductive transformation of nitro compounds by hydrogen sulfide, *Environ. Earth Sci.*, 73 (2015) 1813–1822.
- [25] J. Yu, J. Zou, L. Liu, X. Jiang, F. Jiao, X. Chen, Preparation of TiO_2 based photocatalysts and their photocatalytic degradation properties for methylene blue, rhodamine B and methyl orange, *Desal. Water Treat.*, 81 (2017) 282–290.
- [26] B. Yue, L. Yu, F. Jiao, X. Jiang, J. Yu, The fabrication of pentaerythritol pillared graphene oxide composite and its adsorption performance towards metal ions from aqueous solutions, *Desal. Water Treat.*, 102 (2018) 124–133.
- [27] J. Yang, X. Jiang, F. Jiao, J. Yu, The oxygen-rich pentaerythritol modified multi-walled carbon nanotube as an efficient adsorbent for aqueous removal of alizarin yellow R and alizarin red S, *Appl. Surf. Sci.*, 436 (2018) 198–206.
- [28] J.G. Yu, X.H. Zhao, H. Yang, X.H. Chen, Q. Yang, L.Y. Yu, J.H. Jiang, X.Q. Chen, Aqueous adsorption and removal of organic contaminants by carbon nanotubes, *Sci. Total Environ.*, 482 (2014) 241–251.
- [29] A.K. Geim, K.S. Novoselov, The rise of graphene, *Nat. Mater.*, 6 (2007) 183–191.
- [30] X. Yan, X. Bo, L. Guo, Electrochemical behaviors and determination of isoniazid at ordered mesoporous carbon modified electrode, *Sensor. Actuat. B-Chem.*, 155 (2011) 837–842.
- [31] N. Chen, J. Teng, F. Jiao, X. Jiang, X. Hao, J. Yu, Preparation of triethanolamine functionalized carbon nanotube for aqueous removal of Pb(II), *Desal. Water Treat.*, 71 (2017) 191–200.
- [32] E. Ruiz-Hitzky, M.M.C. Sobral, A. Gómez-Avilés, C. Nunes, C. Ruiz-García, P. Ferreira, P. Aranda, Clay-graphene nanoplatelets functional conducting composites, *Adv. Funct. Mater.*, 26 (2016) 7394–7405.
- [33] R.L.D. Whitby, Chemical control of graphene architecture: tailoring shape and properties, *ACS Nano*, 8 (2014) 9733–9754.
- [34] H. Cui, L. Chen, Y. Dong, S. Zhong, D. Guo, H. Zhao, Y. He, H. Zou, X. Li, Z. Yuan, Molecular recognition based on an electrochemical sensor of per(6-deoxy-6-thio)- β -cyclodextrin self-assembled monolayer modified gold electrode, *J. Electroanal. Chem.*, 742 (2015) 15–22.
- [35] J. Yang, X. Jiang, F. Jiao, J. Yu, X. Chen, Fabrication of diiodocarbene functionalized oxidized multi-walled carbon nanotube and its aqueous adsorption performance toward Pb(II), *Environ. Earth Sci.*, 76 (2017) 677.
- [36] Y.H. Tang, R. Huang, C.B. Liu, S.L. Yang, Z.Z. Lu, S.L. Luo, Electrochemical detection of 4-nitrophenol based on a glassy carbon electrode modified with a reduced graphene oxide/Au nanoparticle composite, *Anal. Methods-UK*, 5 (2013) 5508–5514.
- [37] D. Bhattacharjya, I.Y. Jeon, H.Y. Park, T. Panja, J.B. Baek, J.S. Yu, Graphene nanoplatelets with selectively functionalized edges as electrode material for electrochemical energy storage, *Langmuir*, 31 (2015) 5676–5683.
- [38] X.Q. Cui, X. Fang, H. Zhao, Z.X. Li, H.X. Ren, An electrochemical sensor for dopamine based on polydopamine modified reduced graphene oxide anchored with tin dioxide and gold nanoparticles, *Anal. Methods-UK*, 9 (2017) 5322–5332.
- [39] X.Y. Ma, M.Y. Chao, Z.X. Wang, Electrochemical detection of dopamine in the presence of epinephrine, uric acid and ascorbic acid using a graphene-modified electrode, *Anal. Methods-UK*, 4 (2012) 1687–1692.
- [40] Ö.A. Yokuş, F. Kardaş, O. Akyıldırım, T. Eren, N. Atar, M.L. Yola, Sensitive voltammetric sensor based on polyoxometalate/reduced graphene oxide nanomaterial: Application to the simultaneous determination of l-tyrosine and l-tryptophan, *Sensor. Actuat. B-Chem.*, 233 (2016) 47–54.
- [41] X. Xu, X.Y. Jiang, F.P. Jiao, X.-Q. Chen, J.G. Yu, Tunable assembly of porous three-dimensional graphene oxide-corn zein composites with strong mechanical properties for adsorption of rare earth elements, *J. Taiwan Inst. Chem. E.*, 85 (2018) 106–114.
- [42] C. Li, Z. Wu, H. Yang, L. Deng, X. Chen, Reduced graphene oxide-cyclodextrin-chitosan electrochemical sensor: effective and simultaneous determination of o- and p-nitrophenols, *Sensor. Actuat. B-Chem.*, 251 (2017) 446–454.
- [43] V. Mittal, A.U. Chaudhry, N.B. Matsko, Organic functionalization of thermally reduced graphene oxide nanoplatelets by adsorption: structural and morphological characterization, *Philos. Mag.*, 96 (2016) 2143–2160.
- [44] D. Kumar, K. Singh, V. Verma, H.S. Bhatti, Microwave assisted synthesis and characterization of graphene nanoplatelets, *Appl. Nanosci.*, 6 (2015) 97–103.
- [45] S. Rastgar, S. Shahrokhian, Nickel hydroxide nanoparticles-reduced graphene oxide nanosheets film: Layer-by-layer electrochemical preparation, characterization and rifampicin sensory application, *Talanta*, 119 (2014) 156–163.
- [46] H.L. Tcheumi, I.K. Tonle, E. Ngameni, A. Walcarius, Electrochemical analysis of methylparathion pesticide by a gemini surfactant-intercalated clay-modified electrode, *Talanta*, 81 (2010) 972–979.
- [47] K.J. Chen, C.F. Lee, J. Rick, S.H. Wang, C.C. Liu, B.-J. Hwang, Fabrication and application of amperometric glucose biosensor based on a novel PtPd bimetallic nanoparticle decorated multi-walled carbon nanotube catalyst, *Biosens. Bioelectron.*, 33 (2012) 75–81.
- [48] J. Teng, X. Zeng, X. Xu, J. Yu, Assembly of a novel porous 3D graphene oxide-starch architecture by a facile hydrothermal method and its adsorption properties toward metal ions, *Mater. Lett.*, 214 (2018) 31–33.
- [49] J. Zou, L. Huang, X. Jiang, F. Jiao, J. Yu, Enhanced chiral electrochemical recognition of tryptophan enantiomers using a novel triple-layered GO/BSA/CS modified glassy carbon electrode, *Nanosci. Nanotechnol. Lett.*, 9 (2017) 1700–1707.
- [50] J. Yang, J. Teng, X. Zhao, X. Jiang, F. Jiao, J. Yu, Synthesis, characterization and photocatalytic activities of a novel Eu/ TiO_2 /GO composite, and its application for enhanced photocatalysis of methylene blue, *Nanosci. Nanotechnol. Lett.*, 9 (2017) 1622–1631.
- [51] J.X. Wang, M.X. Li, Z.J. Shi, N.Q. Li, Z.N. Gu, Direct electrochemistry of cytochrome c at a glassy carbon electrode modified with single-wall carbon nanotubes, *Anal. Chem.*, 74 (2002) 1993–1997.
- [52] E. Hammam, A.M. Beltagi, M.M. Ghoneim, Voltammetric assay of rifampicin and isoniazid drugs, separately and combined in bulk, pharmaceutical formulations and human serum at a carbon paste electrode, *Microchem. J.*, 77 (2004) 53–62.